Peer reviewed version

University of Bristol - Explore Bristol Research
General rights

Thickness control of autoclave-moulded composite laminates

Ekaterina Gongadze[*]
Bristol Composites Institute
University of Bristol
Queen's Building, University Walk
Bristol BS8 1TR, UK
Email: kate.gongadze@bristol.ac.uk

Chris Dighton
BAE Systems
Airframe Technology Capability Delivery
Filton, Bristol BS34 7QW, UK
Email: chris.dighton@nccuk.com

Gregory Nash
BAE Systems
Manufacturing, Materials, Strategy and Technology
Samlesbury, Lancashire BB2 7LF, UK

Martin Moss
BAE Systems
Manufacturing, Materials, Strategy and Technology
Samlesbury, Lancashire BB2 7LF, UK

Paul Ainsworth
BAE Systems
Manufacturing, Materials, Strategy and Technology
Samlesbury, Lancashire BB2 7LF, UK

Brett Hemingway
BAE Systems
Manufacturing, Materials, Strategy and Technology
Samlesbury, Lancashire BB2 7LF, UK
Email: behtechsol@gmail.com

Jonathan P.-H. Belnoue
Bristol Composites Institute
University of Bristol
Queen's Building, University Walk
Bristol BS8 1TR, UK
National Composites Centre
Bristol & Bath Science Park
Bristol BS16 7FS, UK
Email: jonathan.belnoue@bristol.ac.uk

Stephen R. Hallett
University of Bristol
Queen's Building, University Walk
Bristol BS8 1TR, UK
Email: stephen.hallett@bristol.ac.uk

[*]Corresponding author.

List of Figures

List of Tables

ABSTRACT

Composite materials and especially those made from pre-impregnated (prepreg) material are widely used in the aerospace industry. To achieve the tight assembly dimensional tolerances required, manufacturers rely on additional manufacturing steps like shimming or machining, which generate extra waste, are time-consuming and expensive. Prepreg sheets come naturally with fibre and resin volume content variability that leads manufacturers to guarantee cured ply thicknesses within a typical +/-5% margin of their nominal values. For thick laminates, this can equate to a thickness variability of as much as a few mm. To solve the issue, it is proposed to twin in-situ laser measurements of the uncured prepreg thickness with numerical simulations of the laminate autoclave consolidation and cure process and to adjust the number of additional sacrificial plies in the laminate based on the model predictions. This reduces the need for expensive and time-consuming trial and error approaches, extra machining operations and results in the production of a part with high accuracy dimensions. Data for IM7/8552 and IM7/977-3 is presented to demonstrate the potential of the method to reach an almost exact target thickness for flat panels.

1 Introduction

The use of fibre reinforced composite materials has been steadily increasing in the aerospace industry for the last 50 years. The variety of resins formulations and reinforcement fibers make them versatile for different requirements and applications. Their excellent low density, high strength and stiffness is however countered by high material and manufacturing costs. The demand to manufacture complex, large and light structures, without employing extensive machining and additional operations requires robust manufacturing processes that can consistently produce high-quality structures, meeting strict tolerance requirements. Modern manufacturing techniques and integration of process models will facilitate waste reduction and attaining Manufacturing 4.0 goals faster, more cost efficiently and in an environmentally sustainable manner. Autoclave processing is the preferred manufacturing method for high-performance parts typically used in aerospace applications. Using this technique, oriented in any direction plies of pre-impregnated (prepreg) carbon fibre materials are stacked to form a component of desired shape and prescribed mechanical properties. After assembly, the structure is covered with layers of cloth - a bleeder to absorb the excess resin and a breather to provide a path for air flow, and sealed inside a vacuum bag (Fig.1a). The tool-laminate assembly is placed in an autoclave, where high temperature and pressure are applied to the laminate in a predetermined cure cycle, to start the resin polymerization. The pressure is applied to compact the laminate to the desired fibre volume fraction and collapse any voids that may develop during the resin cure [5]. Gradually, the fiber permeability decreases, the fiber volume content increases and the laminate thickness decreases until reaching its compaction limit. In the autoclave, the laminate exhibits complex behaviour due to the changing properties of the resin during curing as well as being driven though percolation [6] and shear [7] flow during the consolidation process [8].
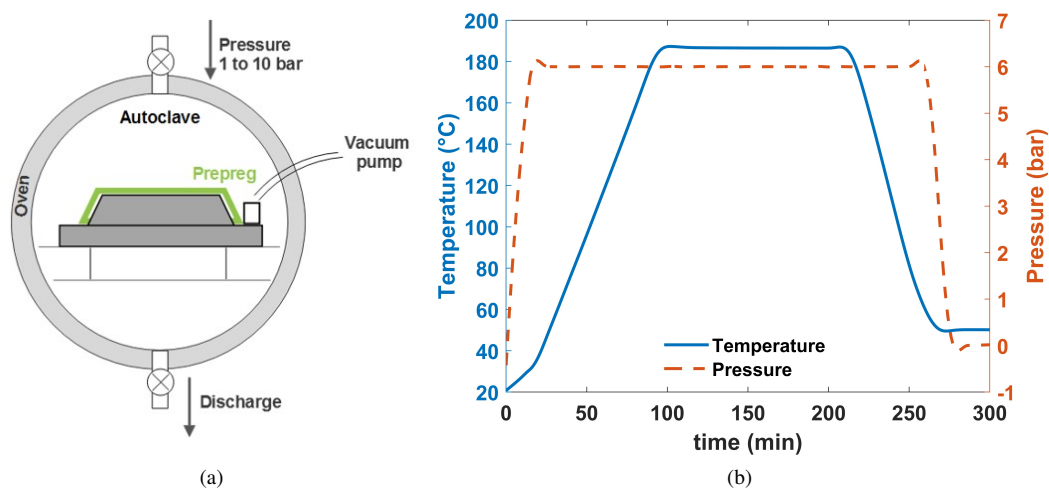

Fig. 1: Typical autoclave set-up a) and the actual cure cycle b) used here to manufacture the IM7/8552 and IM7/977-3 laminates used in the measurements and the simulations.

During the manufacturing process, uncertainties and defects might arise such as fibre misalignment, fibre/ply wrinkling,

bridging and voidage. Ply wrinkling can occur in pre-impregnated materials due to shear interactions between ply and tool [9] as well as forming over complex geometries [10]. [11] showed that complex shapes can cause corner thickening in the early stages of the lay-up and debulking process, followed by wrinkling in the consolidation stage. The severity and frequency of these defects vary depending upon the processing cycle, geometry, tool-part interaction and can significantly influence and compromise the mechanical performance of the composite part. In addition to the direct effects of these features, the effects of variability on the mass properties need to be considered here too, along with fibre straightness of the pre-pregged reinforcements [12]. As pointed out by [13], much of the unidirectional prepreg manufactured today comes with some variability in fibre mass/unit area or resin content, and fibre misalignment already present in the prepreg. A certain amount of variability is due to fibre architecture and resin composition variations generated during production, handling or prepreg storage [14] as well as environmental parameters and autoclave process conditions [15]. Deviation from the nominal thickness, even more pronounced in corners, can also be caused by the geometry and the subsequent differing pressure and the friction between plies too [16]. [17] showed how significant the processing conditions, material systems and their effects on consolidation are. To counteract these issues and meet the required tolerances current part manufacturing practices rely on trial-and-error approaches where an optimal combination of process cycle, tooling and structure design is chosen. To meet tight dimensional constraint, composite parts are often manufactured with sacrificial plies that are machined back later, or shims are added during assembly.

To address this, it is proposed to leverage recent advancements in the simulation of composite laminate autoclave processes and combine these with real-world material thickness variability laser measurements. Being able to measure the uncured prepreg thickness and thus its variability allows to predict the cured ply thickness and simultaneously adjust the number of layers to reach the target thickness for a particular prepreg roll. The modelling framework couples two physical phenomena - cure kinetics and compaction and the heterogeneous nature of the material to predict the number of plies necessary to achieve the required tight tolerances. This paper starts by introducing the modelling framework, where the cure kinetics and the compaction are integrated, followed by the experimental set up and the materials and their properties used to test the models on. Results for Material A (IM7/8552) and Material B (IM7/977-3) are then presented and analysed and the number of plies, needed to achieve the thickness within the tolerance range for different part thicknesses, is recommended. The framework performs very well, and, combined with the simplicity and speed of the code, proves to be a viable tool for smart sustainable manufacturing.

2 Modelling Framework
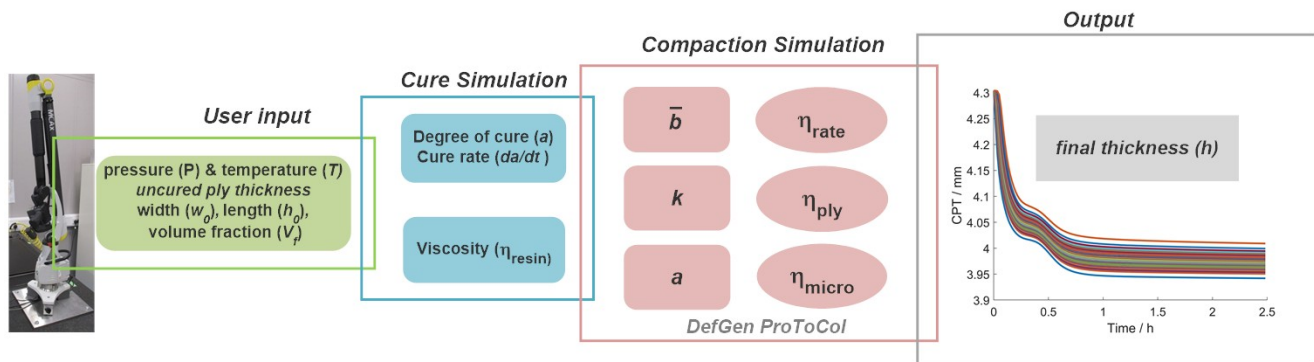
Fig. 2: DefGen ProToCoL workflow with the variability captured by the laser measurements of the uncured part thickness.

The proposed framework is termed the DefGen ProToCoL (Processing Tool for Composite Laminates) (Fig.2) and has the following workflow - input, i.e. measurement of the geometry dimensions and the uncured ply thickness; the respective volume fraction, autoclave pressure and time profiles. The measurements are followed by the simulation part - firstly cure kinetics modelling, where material behaviour, characterised by the degree of cure, cure rate and viscosity is calculated as a function of time and temperature, and secondly consolidation modelling. In the consolidation/compaction part, the cure kinetics output together with physics based model parameters are used to perform the numerical simulation and to generate the final part thickness. To solve the DefGen equations (see Tab.2), an ordinary differential equation solver (ode15s in Matlab) was used and the final thickness is obtained as $h = h_0 e^{\dot{\varepsilon}}$.

Cure Simulations During curing in the autoclave, the thermoset resin goes through two distinctive stages [18]. Initially, liquid-to-rubber transition or gelation occurs, where the resin gradually transforms into a gel state, exhibiting a pure viscous

behaviour and a very slow curing rate. Along with the transformation into the gel state, the curing rate begin to increase rapidly and achieves the maximum rate at the peak conversion. After resin gelation, but prior to vitrification, resin behaviour will be highly viscoelastic. Gradually, vitrification or rubber-to-glass transition takes place where the resin transforms into the glassy state and the curing rate decreases. In the last stage, characterised by elastic behaviour, the curing rate drops noticeably while viscosity increases very rapidly. The time at which this transition occurs depends on the process cycle and the development of resin glass transition temperature (T_g) with the progression of cure.

Table 1: Cure kinetics model equations used in the DefGen ProTocol framework for material IM7/8552 [1] and IM7/977-3 [2].

Cure model for IM7/8552

$$\alpha_{cure} = \frac{\Delta H}{\Delta H_0} \qquad\qquad f = a_f(T - T_g) + b_f \qquad \dot{x}_d = k_{d_0} e^{\frac{B}{f}}$$

$$T_g = T_{g_0} + \frac{(T_{g\infty} - T_{g_0})\lambda\alpha_{cure}}{1 - (1-\lambda)\alpha_{cure}} \qquad\qquad a_f = \begin{cases} a_1 & T_g < T_{g_{a1}} \\ S_a T_g + C_a & T_{g_{a1}} < T_g < T_{g_{a2}} \\ a_2 & T_{g_{a2}} < T_g \end{cases}$$

$$\frac{d\alpha_{cure}}{dt} = \left(\frac{1}{\dot{x}_k} + \frac{1}{\dot{x}_d}\right)^{-1} \qquad\qquad b_f = \begin{cases} b_1 & T_g < T_{g_{b1}} \\ S_b T_g + C_b & T_{g_{b1}} < T_g < T_{g_{b2}} \\ b_2 & T_{g_{b2}} < T_g \end{cases}$$

$$\dot{x}_k = \left(\frac{1}{\dot{x}_{c_1}} + \frac{1}{\dot{x}_{i_2} + \dot{x}_{c_2}}\right)^{-1} + \dot{x}_e \qquad\qquad S_b = \frac{b_2 - b_1}{T_{g_{b2}} - T_{g_{b1}}} \text{ and } C_b = b_2 - S_b T_{g_{b2}}$$

$$\dot{x}_i = K_{0_i} e^{\frac{E_{ai}}{RT}} (1-\alpha)^{l_i} \left(\frac{1}{r} - \alpha\right)^{m_i} (\alpha^{n_{2i}} + b_i)^{n_i} \qquad \eta = \begin{cases} \eta_{0_1} e^{\frac{E_1}{RT}} + \eta_{0_2} e^{\frac{E_2}{RT}} \left(\frac{\alpha_g}{\alpha_g - \alpha_{cure}}\right)^{A + B\alpha_{cure} + C\alpha_{cure}^2} & \eta < \eta_{max} \\ \eta_{max} & \eta \geq \eta_{max} \end{cases}$$

Cure model for IM7/977-3

$$\frac{d\alpha}{dt} = K_1\alpha^3 - K_2\alpha^2 + K_3\alpha + K_4\alpha \qquad\qquad \eta = \eta_\infty \exp(U/RT + B_1\alpha^2 + B_2\alpha)$$

$$K_i = A_i \exp(-\Delta E_i/RT)$$

In general, there are two forms of kinetic models used to describe thermoset curing reactions - empirical and mechanistic models, and their use depends on the type of system and the accuracy of results required. A good overview of those models can be found in [19]. Here, the curing behavior of IM7/8552 was simulated using the well-established model developed by [1]. The equations used to model the degree of cure can be found in Tab.1. The degree of cure, α_{cure}, is related to the enthalpy released during the exothermic reaction of the resin components, where ΔH is the partial heat of reaction at a certain time and ΔH_0 is the total heat of reaction at α is 1. The glass transition temperature can be modelled using the DiBenedetto's equation [20] for a wide variety of thermosets in the form introduced by [21] with T_{g_0} and $T_{g\infty}$ being the glass transition temperature at uncured and fully cured state, respectively. λ is a parameter defined by the difference in heat capacity between glassy and rubber state ($\lambda = 0.435$). In the reaction model, diffusion control is taken into account by the contribution of the kinetic and diffusive rate constants [1]. Viscosity is determined using the relation between temperature and degree of cure, where η_{0_1}, η_{0_2}, E_1, E_2, A, B, C are the model fit parameters with their corresponding values shown in Tab.3. α_g is the degree of cure at gelation and η_{max} is the maximum viscosity and $\lambda = 0.78$.

For IM7/977-3, the cure model and viscosity equations can be found in Tab.1 are based on [2], with similar relations modelled in [22]. A_i are the pre-exponential factors for $i = 1, 2, 3, 4$ ΔE_i are the activation energies, R is the universal constant and T is the absolute temperature. For the viscosity relation, η_∞ is a constant, U is the activating energy for viscosity and B_1 and B_2 are constants independent of temperature.

Compaction Model   As described in the introduction, within the autoclave curing cycle, one of the key physical phenomena that occurs is consolidation. As the pressure gradually increases, plies come into full contact and inter- and intra-ply porosity is eliminated. The resin flow is critical here, as it affects the fibre volume fraction distribution, the appearance of resin rich

or resin poor regions, and ultimately the final dimensions of the part. Two types of flows are observed; (i) percolation, where the fluid can be squeezed and bleed out and (ii) shear flow, where the composite behaves like a viscous fluid with inextensible fibres [5]. Most of the models developed over the years include only one of the two flow types, however [8] and later confirmed by [6] and [23], observed that both flows occur concurrently. Both flows were successfully captured phenomenologically by linking the model parameters to the systems' micro-scale composition by the University of Bristol's DefGen ProToCol model [3] which was validated against experimental data. Recently, the model was further developed to define those parameters that were previously fitting constants as a new physics-based relation [4]. These analytical expressions relate the thickness evolution with time to the applied temperature and pressure cycles, the viscosity of the resin, and meso- and micro- geometrical characteristics of the reinforcements (see Tab.2). The apparent viscosity takes into account coexisting shear and percolation flows and it is a multiplicative decomposition of a strain and a strain rate dependent term. The term η_{strain} can be presented as the product of the deformation at the ply scale (η_{ply}) and at the micro scale (η_{micro}). At the ply scale, the dimensions of the ply are taken into consideration through the width w_0 and height h_0. The deformation through the ply thickness is averaged and the ply experiences through-thickness compaction and in-plane spreading. The transition from squeezing to bleeding flow occurs when shear deformations at the edges reaches a critical level (ε^l). Before locking, the squeezing flow is incompressible i.e. the strain in transverse direction is equal and opposite to the strain in the compaction direction. After locking, the ply is assumed to be fully compressible i.e. no transverse expansion and the volume is lost in bleeding flow. Here, it is taken into account that up to locking the fibre volume fraction does not change and it reaches about 70% in a cured laminate. For thermosets, the temperature of the phase transformation $T_{phtrans}$ and the viscosity $\eta_{phtrans}$ is defined as the temperature at which there is large viscosity drop [4]. For fiber reinforced composites, the microstructure of the reinforcement strongly influences the permeability and the porosity (ε_p) is defined as $V_f = 1 - \varepsilon_p$.

3 Materials and Methods

3.1 Materials

The modelling framework has been extensively tested on thin 4 mm laminates constructed from Material A (HexPly® IM7/8552) [24] and 4, 6 and 8 mm constructed from Material B (CYCOM® IM7/977-3) [25] prepregs. Materials A and B are toughened, high strength, structural epoxy matrices, with unidirectional IM7 (12K) carbon fibres. The recommended manufacturing autoclave cycles are similar for both materials. The autoclave is pressurised to 6 bars and a heat-up cycle is started until 180°C is reached, followed by a 120 min hold at that temperature. Cool down is then initiated until the prescribed

Table 2: The compaction model used in the DefGen ProToCol framework [3; 4].

DefGen ProToCol equations

$$\sigma = \eta_{micro}(\varepsilon)\eta_{ply}(\varepsilon)\eta_{rate}(\dot{\varepsilon})\dot{\varepsilon}$$
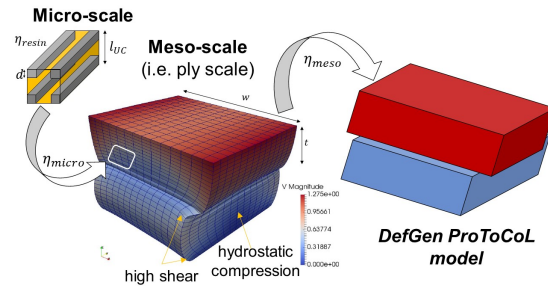
$$\eta_{rate}(\dot{\varepsilon}) = e^{\bar{b}}(-\dot{\varepsilon})^a$$

$$\eta_{ply} = 2\left(\frac{w_0}{h_0}\right)^2 exp(-4\varepsilon)$$

$$\eta_{ply} = 2\left(\frac{w_0}{h_0}\right)^2 exp(-2(\varepsilon+\varepsilon^l))$$

$$\eta_{micro} = 2\eta_{resin}\left(\frac{l_0}{d}\right) exp(\varepsilon)k\left(\frac{k}{\sqrt{\chi_f}exp(\varepsilon)-k}\right)^2$$

$$\eta_{micro} = 2\eta_{resin}\sqrt{\chi_l}exp(\varepsilon)k\left(\left(\frac{k}{\sqrt{\chi_f}exp(\varepsilon)-k}\right)^2+3\right)$$

$\chi_l = exp(-2\varepsilon^l);$ $\quad \chi_f = \frac{4}{3}\chi_l;$ $\quad r_{app} = x + r_{fibre};$ $\quad A_0 = \frac{\pi R^2}{2V_{f0}};$ $\quad A_f = \frac{\pi R^2}{2V_{fmax}};$ $\quad \alpha = \arcsin\left(\frac{A_0}{A_f}\sin\alpha_f\right)$

$\varepsilon^l = -\ln\left(\sqrt{\frac{2}{3}\frac{h_0}{w_0}\tan(\gamma_{lock})+1}\right);$ $\quad \gamma_{lock} = \arcsin\left(\frac{4\frac{A_0}{d^2}-\sin 2\alpha}{1-\cos 2\alpha}\right);$ $\quad \alpha_f = \frac{A_0}{A_0+A_f}\arctan\left(\frac{d}{4A_f}\right)$

$x = r_{fibre}\left(\frac{\sqrt{V_{max}}}{\sqrt{V_f}}-1\right)\tanh\left(\frac{\eta_{resin}}{\eta_{phtrans}}+0.25\right);$ $\quad r_{app} = x + r_{fibre}$

$k = \sqrt{V_{f0}}\left(1-\tanh\left(\frac{\eta_{resin}}{\eta_{phtrans}}+0.25\right)\right)+\sqrt{V_{fmax}}\tanh\left(\frac{\eta_{resin}}{\eta_{phtrans}}+0.25\right)$

$\bar{b} = \left(-16628\left(\frac{T_{phtrans}}{T}\right)+12471\right)\frac{\varepsilon_p^2}{1-\varepsilon_p}r_{app}+\ln(\eta_{resin})$

$a = \frac{m}{R}\frac{1}{T}$

temperature of 50°C is reached and the pressure, which until then was kept constant, is reduced to ambient (Fig.1b).

The parameters used to solve the cure and viscosity equations for Material A and Material B (Tab.1) are presented in Tab.3-4. These constants are based on fitting and interpolating curves to experimental dynamic and isothermal tests. The heat of reaction, H_R, is adopted as 497 J/g (Material A) and 362 J/g (Material B) from [2].

Table 3: Cure and viscosity parameters for HexPly 8552 used in the model [1].

Constants	$\dot{x}_{c_1}$	$\dot{x}_{i_2}$	$\dot{x}_{c_2}$	$\dot{x}_e$	**Cure**		
k_0 [1/s]	153900.5	1000	1000	3.963×10^{11}	$k_{d_0} = 4$ [1/s]	$T_{ga1} = 0$ °C	$b_1 = 0.021$
E_a [J/mol]	64929.5	0	0	133168.3	$a_1 = 4.8 \times 10^{-4}$ [1/°C]	$T_{ga2} = 100$ °C	$b_2 = 0.031$
l	2.347	0	0	1.029	$a_2 = 4.8 \times 10^{-4}$ [1/°C]	$T_{g0} = -7$ °C	$T_{gb1} = 120$ °C
r	1	1	1	1	B = 0.21	$T_{g\infty} = 250$ °C	$T_{gb2} = 195$ °C
m	0	0	0	0	**Viscosity**		
n_2	1	0	0	1	$\eta_{0_1} = 7.5 \times 10^{-11}$ Pa.s	$\alpha_g = 0.545$	A = 2.466
b	0.1594	1	1	0	$\eta_{0_2} = 4.8 \times 10^{-2}$ Pa.s	$E_1 = 81908$ J/mol	B = C = 0
n	1.413	0	0	5.586	$\eta_{max} = 1 \times 10^6$ Pa.s	$E_2 = 13228$	

Table 4: Cure and viscosity parameters for CYCOM 977-3 used in the model [2].

$A_1 = 1.64 \times 10^5$ sec^{-1}	$A_2 = -2.19 \times 10^4$ sec^{-1}
$A_3 = 1.90 \times 10^2$ sec^{-1}	$A_4 = 1.02 \times 10^5$ sec^{-1}
$\Delta E_1 = 6.92 \times 10^4$ J/mol	$\Delta E_2 = 6.00 \times 10^4$ J/mol
$\Delta E_3 = 4.61 \times 10^4$ J/mol	$\Delta E_4 = 7.60 \times 10^4$ J/mol
$K_1 = 11.10$	$K_2 = 0.81$
$\mu_\infty = 3.46 \times 10^{-5}$ Pa s	U $= 4.62 \times 10^4 J/mol$

3.2 Experimental set-up and measurements

Thickness measurements of the uncured and cured thicknesses were performed using a laser metrology apparatus, see Fig.3 at the BAE facility. The laser scanner was a ModelMaker MMDx which incorporates 3rd generation Enhanced Sensor Performance (ESP3) with a digital camera measuring accuracy down to 7 microns.

To benchmark the simulation model, the thickness of three laminates with the same nominal thickness in their uncured and cured state were measured by laser scanning (Tab.4). The dimensions of the laminates were 400 x300 mm , with a nominal thickness of 4.039 mm (32 plies) and a stacking sequence of $\left[+45° / -45° / 0° / 90° \right]_{4S}$. The autoclave curing cycle can be seen in Fig.1b.

Three panels from the same batch of IM7/8552 prepreg were laid up and prepared for measurement (see Fig.4). The panels were vacuum clamped to a granite surface table using a black static intercept vacuum membrane to efficiently reflect the laser light. The panels were laser scanned at 15 points at room temperature, at the debulk and post-cure stages of the process. Each analysis point, located along the panel away from the edges, is a circle with d = 6.35 mm and an area of 10.08 πmm^2, comparable to the size of the micrometer area and results in a data cloud of 200 values. Altogether for each panel, 3000 data points of uncured and cured thickness was available to analyse and generate the histograms in Fig.6.
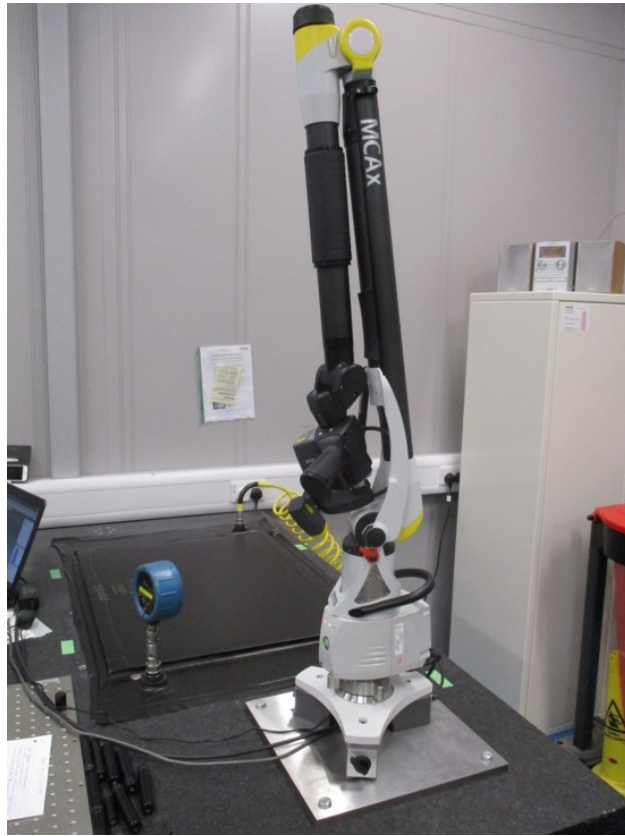
Fig. 3: The laser Nikon Modelmaker MMDX50 MCAx25 used to measure the laminate thickness before and after cure at BAE Systems.

	MDD-11478 - 8552 / IM7 (Batch: 10M0034037A, Roll 006)		
	Panel 1	Panel 3	Panel 5
RT Vac debulk	Yes	Yes	Yes
70 deg C. Vac debulk	Yes		
70 deg C, 100 psi de-bulk		Yes	
Cure	Yes	Yes	Yes
Cure minus peel ply	Yes	Yes	Yes
Co-bond compensation	Yes	Yes	Yes

Fig. 4: Experimental set-up plan for IM7/8552 for a laminate of thickness of 4 mm with each panel from the laminate undergoing different processes.

3.3 Variability

In order to fully model the consolidation process, the inherent material variability of unidirectional carbon epoxy prepreg [12; 13] needs investigating. Prepreg is a sheet of fibres impregnated with resin, which is then pressed and partially cured to produce a flexible raw material ready to be formed to the desired shape and thickness [26]. Each prepreg roll comes with specification limits as defined by the manufacturer (in this case Hexcel) which in turn are based on the client requirements. Typically, the manufacturer measures the resin content, fiber and prepreg areal weights at three points along the length of the roll.

Table 5: Material properties extracted from Certificates of Conformity for 15 batches of HexPly IM7/8552 with their respective resin content (RC), fiber areal weight (FAW), prepreg areal weight (PAW).

Batch	RC [%]	FAW [g/m^2]	PAW [g/m^2]	V_f^*
1	33.06	134.33	200.67	0.596
2	33.98	134.33	203.44	0.586
3	33.37	134.67	202	0.592
4	33.68	134.00	202	0.589
5	33.85	133.83	202.33	0.587
6	32.82	135.00	200.78	0.598
7	33.32	133.67	200.44	0.593
8	33.31	134.78	202.11	0.593
9	33.40	135.00	202.67	0.592
10	32.82	134.83	200.67	0.598
11	33.13	134.33	200.86	0.595
12	33.68	134.83	203.33	0.589
13	33.77	134.00	202.33	0.588
14	33.67	135.33	204	0.589
15	33.60	134.78	202.78	0.59
min	*31.7*	*133*	*197*	*0.573*
mean	*33.4*	*134.4*	*201.9*	*0.591*
max	*35.1*	*137*	*206*	*0.61*
std	*0.65*	*0.89*	*1.96*	

Volume fraction To estimate the volume fraction needed for the computation, historical data available from the certificate of conformity from material supplied to BAE systems over the last three years was examined. 15 batches were reviewed and 111 data points extracted (see Tab. 5). Variability in the mass properties was established, which has been observed in other batches from different manufacturers too [12]. The volume fraction V_f and the CPT of a single ply can be calculated analytically assuming no bleed using the Hexcel reference sheet [27]: $V_f = \frac{\frac{FAW}{\rho_{fibre}}}{\frac{RAW}{\rho_{resin}} + \frac{FAW}{\rho_{fiber}}}$ and $CPT = \frac{FAW}{\rho_{fibre}V_f} x 10$, where ρ_{fibre}=1.788 g/cm^3 and ρ_{resin} = 1.3 g/cm^3 are the fiber and resin densities, respectively. Evaluating the dependency of the calculated cured ply thickness (mm) on the resin content (%) and prepreg areal weight (g/m^2) shows that an increase in those values causes the calculated CPT to increase from 0.123 to 0.131 mm too.

The data from all batches were treated as a single set and the volume fraction distribution can be seen in Fig.5. These data points follow a normal-like distribution and were used as an input in the simulations. Multiple simulations with a nominal cured ply thickness for the 4, 6 and 8 mm laminates and the above obtained normal distribution for the ply volume

fractions were performed, showing insignificant variation in the final thickness. Hence, the uncured plied thickness and the volume fraction variation in the subsequent simulations was fixed at the average value of the normally distributed values.
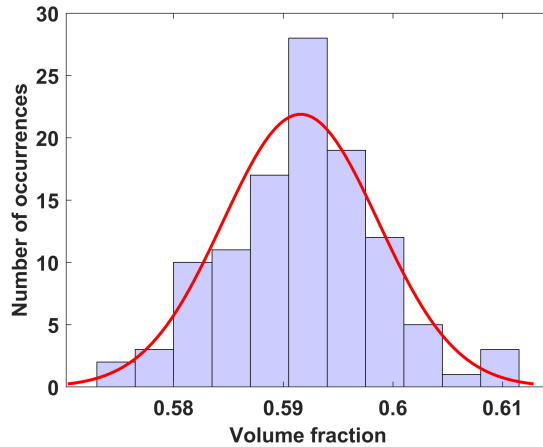

Fig. 5: Histogram of the extracted local distribution of the fibre volume fraction from BAE historical data.

An important point here is that the values of the calculated volume fraction are based on parameters extracted from the cured material, therefore the value should be adjusted for the initial uncured state by multiplying it by a correction factor calculated as $\left(\frac{CPT_{target}}{mean(UCPT)} \right)^2$, which would decrease it by about 15 %.

Thickness The uncured ply thickness for the three panels after room temperature debulk was measured as described in section 3.2 and appeared to follow a normal like distribution which transforms to a left skewed distribution after curing (see Fig.6). The variation in the uncured laminate thickness can be observed between batches (as seen later in Fig.11) as well as within the batch. As the prepreg is delivered and stored in a roll, the core will naturally exhibit greater fibre volume fraction, due to compression from the outer layers and thus a gradient of the thickness will occur along the length of the prepreg tape within a given roll.
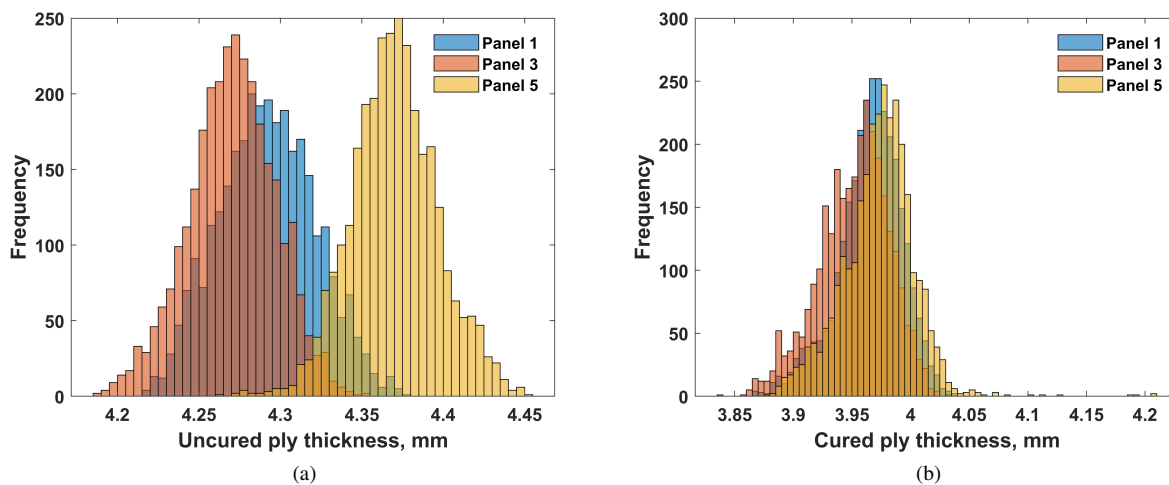

(a)

(b)

Fig. 6: Measured uncured ply thickness (a) and the resulting ply thickness (b) of the 4 mm laminate subject to the predefined autoclave cycle.

4   Results and Discussion
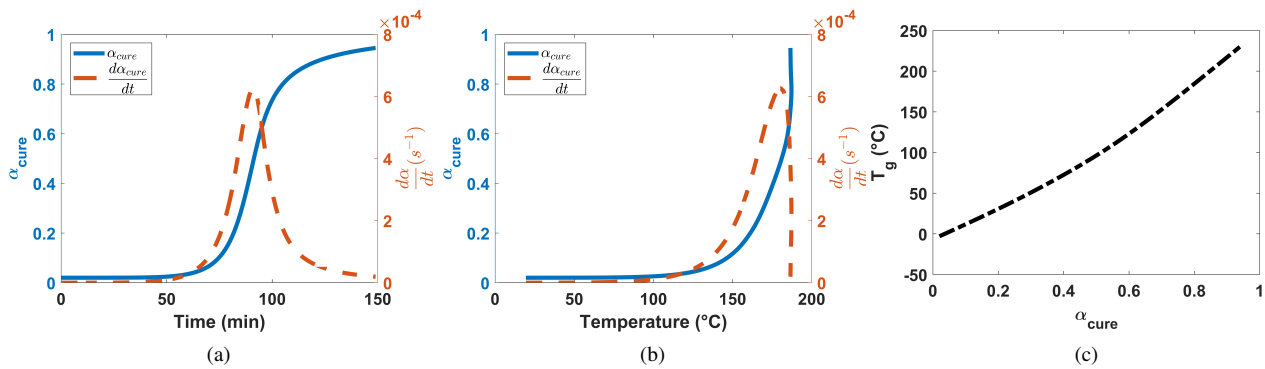
4.1   Degree of cure

(a)

(b)

(c)

Fig. 7: Degree of cure (α_{cure}) and cure rate ($\frac{d\alpha_{cure}}{dt}$) as a function of time (a) and of temperature (b) and the glass transition temperature (T_g) (c) modelled using DiBenedetto equation (for full set of equations used see Tab. 1).

The curing process of thermosetting resins goes through three distinctive stages - gelation (from liquid to rubber), vitrification (from rubber to glass), and crosslinking (reduced molecular mobility and enhanced viscosity). In the initial stage, the curing rate is very slow and after a short period the resin begins to transform into a gel state (Fig.7a). Gradually the curing rate increases rapidly and achieves the maximum rate at the peak conversion. The resin transforms into glassy state (vitrification) leading to a decrease of the curing rate. Finally, the degree of cure reaches above 0.8 and leading to a rapid increase of the viscosity and reaches an effectively infinite value (Fig.8a). At this point further macromolecular reactions will be hindered and the system will be locked. The cure kinetics model used here with the fitted coefficients from [1] was able to show the evolution of the curing rate and degree of cure with time and temperature (Fig.7a and Fig.7b) as well as the glass transition temperature (T_g) as a function of degree of cure α_{cure} (see Fig.7c).
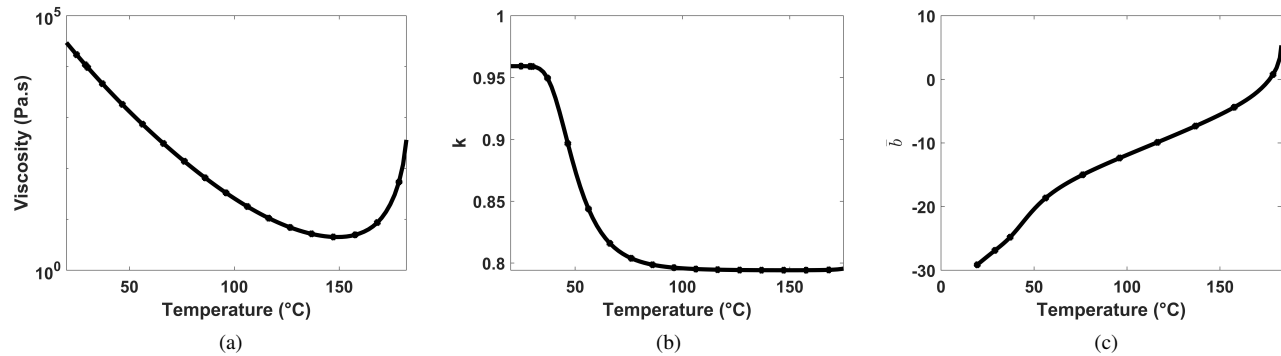

(a)

(b)

(c)

Fig. 8: Evolution of the viscosity η_{resin} (a) and DefGen ProToCol parameters k (b) and $\bar{b}$ (c) with temperature for IM7/8552. The graphs were calculated using the equations presented in Tab. 1 and Tab. 2, respectively.

The evolution with temperature of the DefGen parameter k, which is related to the volume fraction and the structural characteristic of the fibre bed, is presented in Fig.8b. At lower temperatures and hence higher viscosity, the apparent and actual fibres' radii will differ and this was taken into account by normalising the size of the inter-fibre channel. The parameter b (Fig.8c) acts like an energy barrier and controls the flow transition between the squeezing and bleeding flow. The values presented in Fig.8 are in synchrony with the values presented in Tab. 2 in [4].

4.2   Predicted final thickness

Having a closer look at the model, parameter b, as a function of temperature shows a steadily decreasing value with increasing temperature. Similar behaviour was observed for parameter k with initially the parameter decreasing until the

cure rate picks up at 100°C, where after k remains constant. The consolidation behaviour of the laminate was analysed and good agreement with the measured data was observed. Looking closely at the development of the thickness over time, the laminate reaches its compaction limit after 1 hour in the autoclave.
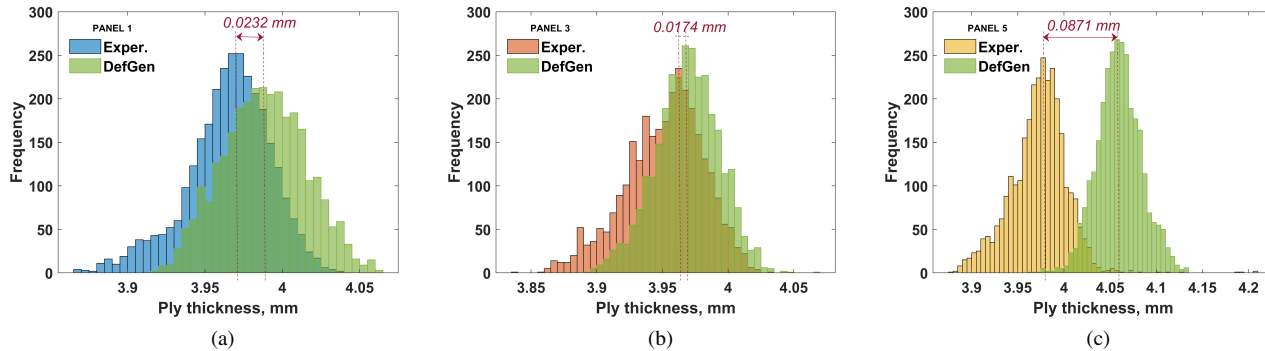

(a)　　　　　　　　　　　　(b)　　　　　　　　　　　　(c)

Fig. 9: Measured and simulated cured ply thickness for IM7/8552 Panel 1 (a), 3 (b) and 5 (c) using the uncured normal distribution and an averaged corrected volume fraction.

The histograms of cured thickness, predicted from the uncured measurements for the IM7/8552 panels 1, 3 and 5 are presented in Fig.9, where the simulations can be seen to capture the distribution profile and behaviour of the experimental results very well. The difference in the mean values is only at a level of 10s of microns, i.e. 0.02, 0.01 and 0.08 mm for panel 1, 3 and 5 respectively.
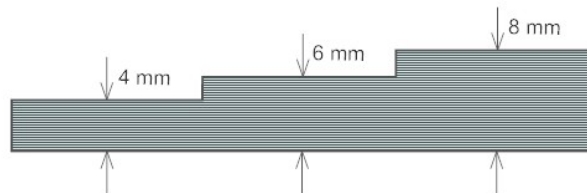

Fig. 10: Stepped laminate of a 4 mm, 6 mm and 8 mm thickness.

Stepped laminate The model was also applied to IM7/977-3 using the equations (Tab.1) and parameters (Tab.4) presented in the previous sections. 4, 6 and 8 mm thick sections (see Fig.10) were modelled using data from two batches of pre-preg material, with simulated autoclave processing conditions as described in Fig.1b. The framework was able to predict all three thicknesses from the first batch particularly well, as shown in Fig.11. The uncured laminates from the second batch were slightly thicker and the degree of compaction was on average 8% (4 mm) and 6.5 % (6 and 8 mm). The degree of compaction however is consistent across all laminates and averages around 5.5%. The experimental measurements show that the 4-mm has the largest compaction with 8%, whereas the 6th and 8th have an average of 5.5%. The latter could be explained by the way the sample laminates were vacuum bagged and formed a step like part showing the need of a 3D model to capture complex geometries and additional influences.

To answer the question of how many plies a part needs in order to reach a required target thickness, the model was applied to a stepped IM7/8552 laminate panel, with sections of 4, 6 and 8 mm thickness (see Fig.10). To achieve a typical tolerance range of +/-0.1 mm for the material data used in this paper, in the 4 mm section, an additional ply is advisable over and above the nominal design, but for the 6 and 8 mm sections it is completely necessary in order to bring the panel precisely to the target thickness. For the 8mm section even 2 additional plies could still be within the tolerance range (Fig.12).

5 Conclusion

This study addresses the challenge of thickness control during compaction of flat multi-layer prepreg laminates in an autoclave environment. The manufacturing industry typically relies on additional manufacturing steps, which generate
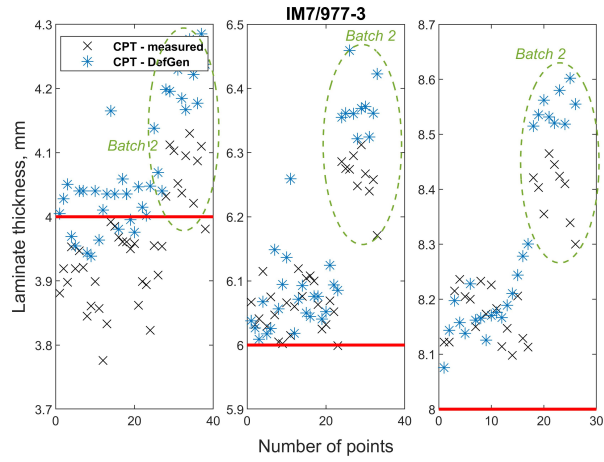
Fig. 11: Measured and simulated cured ply thickness for a 4 mm, 6 mm and 8 mm laminate using IM7/977-3 material. The red line shows the target thickness for each panel respectively.
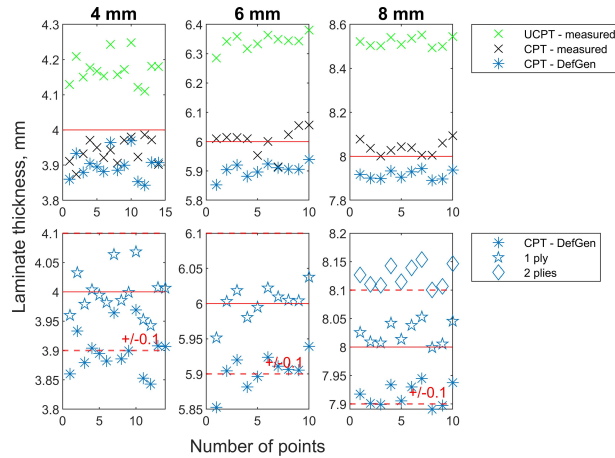

Fig. 12: Measured uncured and cured ply thickness and DefGen cured ply thickness for a 4 mm, 6 mm and 8 mm laminate. The red line shows the target thickness for each panel respectively.

waste and are time and resource consuming. Here, we propose using in-situ measurement of the uncured laminate, which would capture the real-world thickness variability of the prepreg material, and the predefined fibre volume as input to a process model, where the part cure and consolidation is simulated to predict its final thickness. The result is a fast output which enables real time feedback so that the number of plies can be adjusted to ensure that the final thickness lies within the required tolerance range. To summarise, for processes where the thickness of the final part and the number of plies required to achieve such thickness is important, the model presented here, combining cure kinetics, compaction and material variability, is able to provide accurate results. A future next step would be to test the numerical model against more complex geometries. Parts with complex geometries are commonly subjected to corner thickening/thinning at curvature locations and hence deviating from the expected nominal thickness. The pressure at these regions differs and the friction between the mould and the laminates restricts the conformity. The result is resin rich/poor regions, porosity, fibre wrinkling and ultimately decreased mechanical performance. This would necessitate the use of fast 3D numerical models such as the one recently proposed by [10]. The proposed method will facilitate creation of waste-free and sustainable manufacturing steps and a symbiosis between data analysis, numerical simulations and real-time measurements.

References

[1] van Ee, D., and Poursartip, A., 2009. Hexply 8552 material property database for use with compro cca and raven. Techreport.

[2] Ng, S., Boswell, R., Claus, S., Arnold, F., and Vizzini, A., 2000. Degree of cure, heat of reaction, and viscosity of 8552 and 977-3 hm epoxy resin. Techreport, Naval Air Warfare Center Aircraft Division.

[3] Belnoue, J., Nixon-Pearson, O. J., Ivanov, D., and Hallett, S. R., 2016. "A novel hyper-viscoelastic model for consolidation of toughened prepregs under processing conditions". *Mechanics of Materials,* **97**, pp. 118–134.

[4] Belnoue, J. P.-H., Valverde, M. A., Onoufriou, M., Sun, X. R., Ivanov, D. S., and Hallett, S. R., 2021. "On the physical relevance of power law-based equations to describe the compaction behaviour of resin infused fibrous materials". *International Journal of Mechanical Sciences,* **199**, p. 106425.

[5] Hubert, P., and Poursartip, A., 1998. "A review of flow and compaction modelling relevant to thermoset matrix laminate processing". *Journal of Reinforced Plastics and Composites,* **17**(4), pp. 286–318.

[6] Sorba, G., Binetruy, C., Leygue, A., and Comas-Cardona, S., 2017. "Squeeze flow in heterogeneous unidirectional discontinuous viscous prepreg laminates: Experimental measurement and 3d modeling". *Composites Part A: Applied Science and Manufacturing,* **103**, pp. 196–207.

[7] Engmann, J., Servais, C., and Burbidge, A. S., 2005. "Squeeze flow theory and applications to rheometry: A review". *Journal of Non-Newtonian Fluid Mechanics,* **132**(1), pp. 1–27.

[8] Hubert, P., and Poursartip, A., 2001. "Aspects of the compaction of composite angle laminates: An experimental investigation". *Journal of Composite Materials,* **35**(1), pp. 2–26.

[9] Lightfoot, J. S., Wisnom, M. R., and Potter, K., 2013. "A new mechanism for the formation of ply wrinkles due to shear between plies". *Composites Part A: Applied Science and Manufacturing,* **49**, pp. 139–147.

[10] Belnoue, J. P.-H., and Hallett, S. R., 2020. "A rapid multi-scale design tool for the prediction of wrinkle defect formation in composite components". *Materials Design,* **187**, p. 108388.

[11] Netzel, C., Mordasini, A., Schubert, J., Allen, T., Battley, M., Hickey, C., Hubert, P., and Bickerton, S., 2021. "An experimental study of defect evolution in corners by autoclave processing of prepreg material". *Composites Part A: Applied Science and Manufacturing,* **144**, p. 106348.

[12] Potter, K., Langer, C., Hodgkiss, B., and Lamb, S., 2007. "Sources of variability in uncured aerospace grade unidirectional carbon fibre epoxy preimpregnate". *Composites Part A: Applied Science and Manufacturing,* **38**(3), pp. 905–916.

[13] Potter, K., Khan, B., Wisnom, M., Bell, T., and Stevens, J., 2008. "Variability, fibre waviness and misalignment in the determination of the properties of composite materials and structures". *Composites Part A: Applied Science and Manufacturing,* **39**(9), pp. 1343–1354.

[14] Mesogitis, T., Skordos, A., and Long, A., 2014. "Uncertainty in the manufacturing of fibrous thermosetting composites: A review". *Composites Part A: Applied Science and Manufacturing,* **57**, pp. 67–75.

[15] Baran, I., Cinar, K., Ersoy, N., Akkerman, R., and Hattel, J. H., 2017. "A review on the mechanical modeling of composite manufacturing processes". *Arch Computat Methods Eng,* **24**, p. 365–395.

[16] Levy, A., and Hubert, P., 2019. "Vacuum-bagged composite laminate forming processes: Predicting thickness deviation in complex shapes". *Composites Part A: Applied Science and Manufacturing,* **126**, p. 105568.

[17] Matveev, M., Belnoue, J.-H., Nixon-Pearson, O., Ivanov, D., Long, A., Hallett, S., and Jones, I., 2019. "A numerical study of variability in the manufacturing process of thick composite parts". *Composite Structures,* **208**, pp. 23–32.

[18] Lange, J., Altmann, N., Kelly, C., and Halley, P., 2000. "Understanding vitrification during cure of epoxy resins using dynamic scanning calorimetry and rheological techniques". *Polymer,* **41**(15), pp. 5949 – 5955.

[19] Halley, P. J., and Mackay, M. E., 1996. "Chemorheology of thermosets—an overview". *Polymer Engineering & Science,* **36**(5), pp. 593–609.

[20] DiBenedetto, A. T., 1987. "Prediction of the glass transition temperature of polymers: A model based on the principle of corresponding states". *Journal of Polymer Science Part B: Polymer Physics,* **25**(9), pp. 1949–1969.

[21] Nielsen, L., 1968. Crosslinking-effect on physical properties of polymers. Techreport, Monsanto Research Corporation.

[22] Mantell, S. C., Ciriscioli, P. R., and Almen, G., 1995. "Cure kinetics and rheology models for ici fiberite 977-3 and 977-2 thermosetting resins". *Journal of Reinforced Plastics and Composites,* **14**(8), pp. 847–865.

[23] Hautefeuille, A., Comas-Cardona, S., and Binetruy, C., 2019. "Mechanical signature and full-field measurement of flow-induced large in-plane deformation of fibrous reinforcements in composite processing". *Composites Part A: Applied Science and Manufacturing,* **118**, pp. 213–222.

[24] Hexcel, 2020. Product data sheet.

[25] Solvay, 2020. Product data sheet.

[26] Hull, D., and Clyne, T., 1996. *An Introduction to Composite Materials*. Cambridge University Press.

[27] Hexcel, 2013. Hexply® prepreg technology.